Cooperative and Dynamically Weighted Model Predictive Control of a 3-Level Uninterruptible Power Supply With Improved Performance and Dynamic Response

Luís M. A. Caseiro, *Member, IEEE*, André M. S. Mendes, *Member, IEEE*, and Sérgio M. A. Cruz, *Senior Member, IEEE*

***Abstract*—In this paper, we propose a 3-level double conversion uninterruptible power supply with a new cooperative and dynamically weighted model predictive control technique. A 3-level dc–dc converter is used to improve the dc bus balance and the overall response of the uninterruptible power supply (UPS). A new cooperative model predictive control principle is proposed to enhance the response of multiconverter systems. New controllers are proposed for all converters of the UPS, based on the dynamically weighted model predictive control technique and using the presented cooperative principle. A new power management technique is also proposed for the UPS. The proposed 3-level UPS system presents improved dynamic response and steady-state performance in distinct operating points, when compared to the conventional system. Experimental results demonstrate the advantages of each proposed novelty.**

***Index Terms*—Neutral-point-clamped (NPC), optimal switching vector model predictive control (OSV-MPC), predictive control, uninterruptible power supply (UPS).**

I. Introduction

UNINTERRUPTIBLE power supplies (UPS) are crucial in critical applications, protecting the load from grid faults and disturbances. Hence, it is important to improve the performance and reliability of these systems.

Multilevel converters are largely used in industrial systems, especially the neutral-point-clamped (NPC) topology [1]. However, even though multilevel converters are frequently used in the ac–dc stages of UPSs, conventional dc–dc topologies are still typically used to interface with the battery bank. In this paper, a 3-level dc–dc (3LDC) converter is used in the UPS system, in addition to two 3-level NPC (3LNPC) converters, improving dc bus capacitor balancing.

Model predictive control (MPC) has proven to be an excellent control solution for power electronics [2], with optimal switching vector MPC (OSV-MPC) being the most popular type of MPC in this field. Despite recent advances, OSV-MPC still presents important challenges, such as weighting factor (WF) selection or its high computational load [2].

The computational burden of OSV-MPC is particularly steep when it is used in systems with multiple interconnected converters, especially if these are multilevel converters. In such cases, a single OSV-MPC controller can be used to control the whole system, but this exponentially increases the complexity of the controller, hindering its real-time feasibility. To avoid this, each converter is typically controlled independently [3]–[6]. However, this means each controller overlooks the impact of the remaining converters [3]–[5] or considers only their past actions [6], leading to a nonoptimal control action.

This paper proposes a new cooperative control principle, which improves multiconverter response, with the same computational effort as the fully independent solution. In the studied UPS, this technique improves dc bus capacitor balance, as well as the overall steady-state performance.

Another significant problem of OSV-MPC is WF selection. Since no analytical methods exist for the selection of optimal WFs [2], one must typically rely on extensive simulation and testing to find the values that produce optimal results in a given operating point (according to the chosen performance criteria) [2], [7]–[9]. In addition, different operating points require different WFs to achieve optimal performance [8]–[10]. Hence, the chosen WFs must inherently compromise performance in some operating conditions in order to improve it in others. Moreover, WFs also affect the dynamic response [8], [10], so WFs selected for optimal steady-state operation cannot always ensure an adequate dynamic response (as shown in this paper).

In light of these problems, some techniques avoid the use of WFs [11]–[14], but while these avoid the problem of

Manuscript received August 6, 2018; revised November 29, 2018, March 1, 2019, and April 23, 2019; accepted May 17, 2019. Date of publication June 25, 2019; date of current version February 10, 2020. This work was supported in part by the Project SAICT-45-2017-POCI-01-0145-FEDER-029112 - PTDC/EEI-EEE/29112/2017, funded by "Programa Operacional Temático Competitividade e Internacionalização" – FEDER and by the Foundation for Science and Technology (FCT)—OE, and in part by the Project UID/EEA/50008/2019, funded by FCT–OE. *(Corresponding author: Luís M. A. Caseiro.)*

The authors are with the Instituto de Telecomunicações, 1049-001 Lisbon, Portugal, and also with the Department of Electrical and Computer Engineering, University of Coimbra, 3030-290 Coimbra, Portugal (e-mail: lcaseiro@ieee.org; amsmendes@ieee.org; smacruz@ieee.org).

Color versions of one or more of the figures in this paper are available online at http://ieeexplore.ieee.org.

Digital Object Identifier 10.1109/TIE.2019.2921283

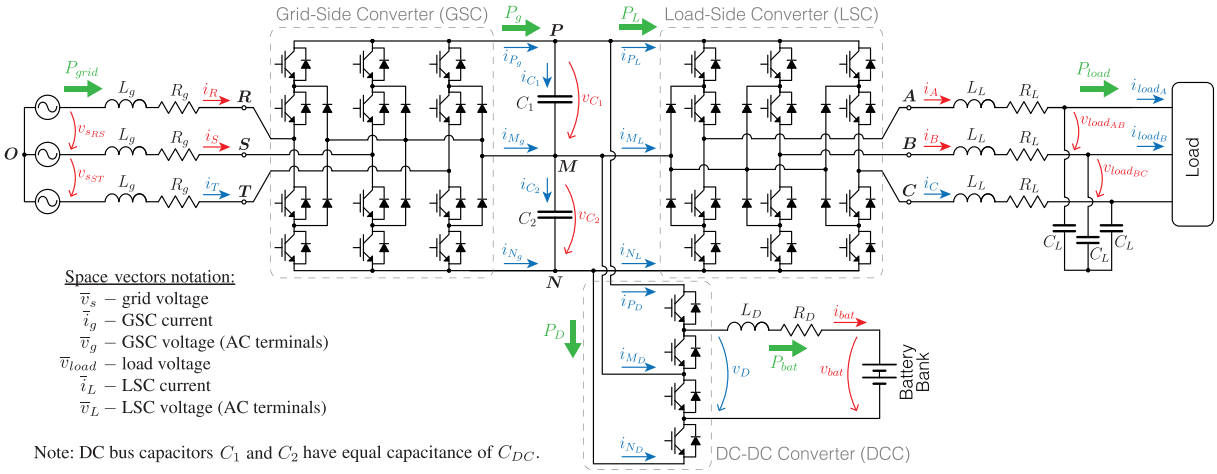

Fig. 1. Circuit of the proposed 3-level double conversion UPS system, relevant signals (measured signals shown in red) and power flow (in green).

parameter selection, they still impose a fixed weight relation between objectives, limiting performance in different conditions. Ranking-based approaches [15], [16] also avoid WFs, but lose sensitivity in regard to error magnitude (i.e., for each objective, the controller only knows that a given control option produces a lower error than another, but not the difference in error amplitude).

In order to optimize OSV-MPC performance in varying conditions, some solutions have been proposed to adjust the WFs during operation [10], [17]–[21]. However, most of these techniques have important drawbacks, such as being limited to a specific system with specific objectives [17], [18], requiring extensive training [19] or providing a discontinuous WF variation [20], [21]. The dynamically weighted OSV-MPC (DWMPC) technique, proposed in [10], provides an analytic approach for the continuous real-time adjustment of WFs. This technique allows the controller to adapt to different operating conditions, improving both the steady-state performance and dynamic response.

This paper proposes a cooperative DWMPC (Co-DWMPC) UPS control system, combining the presented cooperative control principle with new DWMPC controllers for all converters of the UPS system. The DWMPC controllers complement the cooperative principle, defining a hierarchy regarding the common objective. This improves both the dc bus capacitor balance and other UPS parameters (load voltage and grid current). These techniques ensure high converter cooperation and control adaptability, improving steady-state performance at different operating points and the overall dynamic response.

A new power management system (PMS) based on the UPS power balance is also proposed, providing faster transient response than conventional proportional-integral (PI) controllers, with no overshoot, and very little design effort. This solution also provides low grid current distortion, even with highly nonlinear loads, and uses the dc–dc converter to aid in (dis)charging the dc bus.

In summary, this paper has three main contributions, which are as follows.

1) A new cooperative OSV-MPC principle, for improved multiconverter performance, with low computing cost.
2) New OSV-MPC controllers for all converters of the UPS, based on the DWMPC technique and the new cooperative principle.
3) A new UPS PMS, with very fast dynamic response and good steady-state performance.

The proposed control system provides improved UPS steady-state performance and dynamic response when compared to conventional OSV-MPC and PI-based solutions.

The studied UPS system is presented in Section II. An overview of the proposed control system is presented in Section III, including the new PMS. The conventional OSV-MPC controllers, used for comparison, are presented in Section IV. The principle of cooperative OSV-MPC is proposed in Section V and the proposed Co-DWMPC controllers are given in Section VI. Finally, experimental results demonstrating the merits of each proposal are presented in Section VII, and Section VIII concludes this paper.

II. Studied System and Mathematical Model

In this paper, a 3-level double conversion UPS system is proposed, consisting of two 3LNPC converters and a 3LDC converter sharing a single dc bus, as represented in Fig. 1.

All 3-phase signals are studied in the $\alpha\beta$ reference frame. The space vector of each 3-phase variable x is given by

$$\overline{x} = x_\alpha + j x_\beta = \frac{2}{3}\left(x_R + a\, x_S + a^2\, x_T\right) \tag{1}$$

where $a = e^{j\frac{2\pi}{3}}$. On the load-side, R, S, T are replaced with A, B, C. The used space vector notation is shown in Fig. 1. Each 3LNPC converter has three possible switching states S_X in each phase X ($S_X \in \{-1, 0, 1\}$), which produce pole voltage values $v_{XM} \in \{-v_{C_2}, 0, v_{C_1}\}$, respectively. The three phases are represented by $X \in \{R, S, T\}$ on the grid-side converter (GSC) and by $X \in \{A, B, C\}$ on the load-side converter (LSC). The voltage at the ac terminals of the GSC and LSC (analogous) is given, in space vector format, by

$$\overline{v}_g = v_{g_\alpha} + j v_{g_\beta} = \frac{2}{3}\left(v_{RM} + a\, v_{SM} + a^2\, v_{TM}\right). \tag{2}$$

The grid-side and load-side circuit dynamics are given by

$$\frac{d\bar{i}_g}{dt} = -\frac{R_g}{L_g}\bar{i}_g + \frac{1}{L_g}\bar{v}_s - \frac{1}{L_g}\bar{v}_g \tag{3}$$

$$\begin{cases} \frac{d\bar{i}_L}{dt} = -\frac{R_L}{L_L}\bar{i}_L - \frac{1}{L_L}\bar{v}_{\text{load}} + \frac{1}{L_L}\bar{v}_L \\ \frac{d\bar{v}_{\text{load}}}{dt} = \frac{1}{C_L}\bar{i}_L - \frac{1}{C_L}\bar{i}_{\text{load}} \end{cases}. \tag{4}$$

The dc–dc converter (DCC) has four possible switching states, $S_D \in \{0,1,2,3\}$, which produce voltage values $v_D \in \{0, v_{C_1}, v_{C_2}, v_{dc}\}$, respectively. The battery current dynamics is given by

$$\frac{di_{\text{bat}}}{dt} = -\frac{R_D}{L_D}i_{\text{bat}} - \frac{1}{L_D}v_{\text{bat}} + \frac{1}{L_D}v_D\ . \tag{5}$$

The behavior of the dc bus capacitors is modeled by

$$\frac{dv_{C_n}}{dt} = \frac{1}{C_{\text{dc}}}i_{C_n}, \quad n = 1,2 \tag{6}$$

$$\begin{cases} i_{C_1} = i_{P_g} - i_{P_L} - i_{P_D} = i_{C_2} - i_{M_g} + i_{M_L} + i_{M_D} \\ i_{C_2} = -i_{N_g} + i_{N_L} + i_{N_D} = i_{C_1} + i_{M_g} - i_{M_L} - i_{M_D} \end{cases} \tag{7}$$

$$\begin{cases} i_{P_g} = i_R\,(S_R = 1) + i_S\,(S_S = 1) + i_T\,(S_T = 1) \\ i_{M_g} = i_R\,(S_R = 0) + i_S\,(S_S = 0) + i_T\,(S_T = 0) \\ i_{N_g} = i_R\,(S_R = -1) + i_S\,(S_S = -1) + i_T\,(S_T = -1) \end{cases} \tag{8}$$

$$\begin{cases} i_{P_D} = i_{\text{bat}}\,((S_D = 1) + (S_D = 3)) \\ i_{M_D} = -i_{\text{bat}}\,(S_D = 1) + i_{\text{bat}}\,(S_D = 2) \\ i_{N_D} = -i_{\text{bat}}\,((S_D = 2) + (S_D = 3)) \end{cases} \tag{9}$$

where $(S_X = n)$ is 1 if S_X has value n and 0 otherwise. $i_{P_L}, i_{M_L}, i_{N_L}$ are calculated analogously to (8).

III. Proposed UPS Control System

The proposed UPS control system is schematically represented in Fig. 2. At each sampling instant k, the signals shown in red in Fig. 1 are measured. As usual, a one-step prediction is used to account for the calculation time of the control algorithm. Hence, the system state at $k+1$ is estimated considering the switching states applied at k. The predictive controllers then select the action that minimizes a given cost function at $k+2$ (discussed in the next sections).

A. System State Prediction at $k+1$

Using the forward Euler method, the grid-side current at $k+1$ is predicted using

$$i^p_{g_\alpha}[k+1] = \left(1 - \frac{R_g T_s}{L_g}\right) i_{g_\alpha}[k] + \frac{T_s}{L_g}v_{s_\alpha}[k] - \frac{T_s}{L_g}v_{g_\alpha}[k]\,. \tag{10}$$

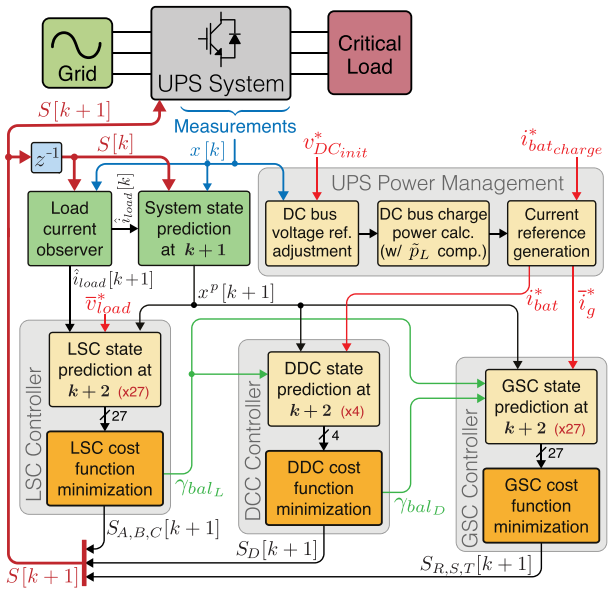

Fig. 2. Schematic representation of the proposed UPS controller, with a novel PMS and cooperative DWMPC controllers.

The load-side filter model is considered in state-space form, as described in [22], leading to

$$\begin{bmatrix} i^p_{L_\alpha} \\ v^p_{\text{load}_\alpha} \end{bmatrix}[k+1] = \mathbf{A}\begin{bmatrix} i_{L_\alpha} \\ v_{\text{load}_\alpha} \\ \hat{i}_{\text{load}_\alpha} \end{bmatrix}[k] + \mathbf{B}v_{L_\alpha}[k] \tag{11}$$

$$\mathbf{A} = \begin{bmatrix} A_{11} & A_{12} & A_{13} \\ A_{21} & A_{22} & A_{23} \end{bmatrix}, \quad \mathbf{B} = \begin{bmatrix} B_1 \\ B_2 \end{bmatrix} \tag{12}$$

where $\mathbf{A}$, $\mathbf{B}$ are the discrete state-space matrices and $\hat{i}_{\text{load}}[k]$ is the estimated load current, obtained using an observer [22]. Similar equations are used for the β components. The battery current and dc bus capacitor voltages are predicted by

$$i^p_{\text{bat}}[k+1] = \left(1 - \frac{R_D T_s}{L_D}\right) i_{\text{bat}}[k] - \frac{T_S}{L_D}v_{\text{bat}}[k] + \frac{T_S}{L_D}v_D[k] \tag{13}$$

$$\begin{cases} v^p_{C_1}[k+1] = v_{C_1}[k] + \frac{T_s}{C_{\text{dc}}}i_{C_1}[k] \\ v^p_{C_2}[k+1] = v_{C_2}[k] + \frac{T_s}{C_{\text{dc}}}i_{C_2}[k] \end{cases} \tag{14}$$

where $i_{C_1}[k]$ and $i_{C_2}[k]$ are calculated using (7)–(9).

B. UPS Power Management

In a UPS system, the current references are typically obtained using a PI controller. Even though this provides zero steady-state error, its dynamic response is not always satisfactory and its tuning can be difficult. For this reason, a new power management algorithm is proposed. Based on the UPS power balance, the grid power reference is given by

$$P^*_{\text{grid}} = (P_{\text{grid}} - P_g) + P_L + (P^*_{\text{bat}} + (P_D - P_{\text{bat}})) + P^*_{\text{charge}} \tag{15}$$

where P_{grid} is the active power currently drawn from the grid, P_{load} is the active power supplied to the load, P_{bat} is the power supplied to the batteries and P_g, P_L, P_D are the active powers supplied/drawn by each converter to/from the dc bus (shown in Fig. 1). P^*_{charge} represents the power required to charge/discharge the dc bus to the reference voltage in a horizon of N_{charge} samples [6], [10]. From [6], [10] P^*_{charge} is typically given by

$$P^*_{\text{charge}} = \frac{C_{\text{dc}}\left(v^{*2}_{\text{dc}} - v^2_{\text{dc}}\right)}{4N_{\text{charge}} \cdot T_s} \tag{16}$$

and functions similarly to a feed-forward term. As shown in [6] and [10], this approach provides excellent results when used with linear loads. However, when the UPS supplies a nonlinear load, the instantaneous power drawn from the dc bus by the LSC, p_L, has a highly oscillating component $\tilde{p}_L = p_L - P_L$, which leads to a steady-state dc bus voltage oscillation. With the formulation in (16), P^*_{charge} reflects this oscillation, leading to an oscillating P^*_{grid} and significant grid current distortion. To avoid this, a new P^*_{charge} formulation is now proposed, overlooking the effect of the oscillating power component $\tilde{p}_L$. Hence, P^*_{charge} is given by

$$P^*_{\text{charge}} = \frac{C_{\text{dc}}\left(v^{*2}_{\text{dc}} - v^2_{\text{dc}}\right)/4 - \text{int}\left(\tilde{p}_L\right)}{N_{\text{charge}} \cdot T_s} \tag{17}$$

where $\text{int}\left(\tilde{p}_L\right)$ is the discrete integral of $\tilde{p}_L$. The dc component of the integral is overlooked. This term represents the energy drawn from the dc bus due to $\tilde{p}_L$. With this formulation, the PMS overlooks the dc bus voltage oscillation caused by the nonlinearity of the load, ensuring sinusoidal grid currents at any load condition.

This approach provides very fast voltage tracking with no overshoot and very little design effort. The only design parameter is the charging horizon N_{charge}, which defines the response time of the system. For example, $N_{\text{charge}} = 80$ with $T_s = 70\ \mu$s means the PMS always aims to (dis)charge the dc bus in 5.6 ms. The main disadvantage of this technique is the possibility of a steady-state error, due to power estimation inaccuracies. However, a small dc bus voltage deviation has no significant impact on the UPS operation.

The grid current references ($\vec{i}^*_g$) are calculated using P^*_{grid} and the grid voltage phase, given by a phase-locked loop (PLL). To avoid over-currents, the current references are limited to their nominal value whenever they surpass it. When this happens, the GSC is unable to supply all required power P^*_{grid}, so the DCC is called upon to supply the difference. The battery current needed to complement the GSC power is subtracted from the charging current given by the battery management system ($i^*_{\text{bat}_{\text{charge}}}$), resulting in the battery current reference (i^*_{bat}). This strategy requires no tuning and is valid for all UPS operation modes, so no transition between modes is needed. Additionally, the DCC can aid the GSC in all UPS modes (to compensate grid unavailability, undervoltages, sags, disturbances, etc.).

Power converter components, such as capacitors and insulated gate bipolar transistors (IGBTs), can be easily damaged by overvoltages. Hence, it is important to ensure that the dc bus capacitors do not exceed a maximum voltage threshold. Since the power reference considers only the total dc voltage, the UPS can actually overcharge one of the capacitors when these are unbalanced. To avoid this, the dc bus voltage reference is adjusted as

$$v^*_{\text{dc}} = \min\left(v^*_{\text{dc}_{\text{init}}}, 2v_{C_{\max}} - |\Delta v_C|\right) \tag{18}$$

where $\Delta v_C = v_{C_1} - v_{C_2}$. This way, when the capacitors are unbalanced, the controller only charges them until the one with the highest voltage reaches $v_{C_{\max}}$ (avoiding overvoltages).

IV. Conventional OSV-MPC Controllers

Given the predicted system state at $k+1$ and the calculated references, the controller of each UPS converter selects the control action (to be applied at $k+1$) that minimizes a given cost function at $k+2$. This section presents the conventional OSV-MPC controller formulation for each converter. This formulation is then used as the base for the deduction of the new DWMPC controllers in Section VI and for comparison in the experimental results.

A. Grid-Side Controller

The grid-side controller considers two objectives: the minimization of the grid current vector error (g_{i_g}); and the balancing of the dc bus capacitor voltage (g_{bal_g}). The global grid-side controller cost function is

$$G_g = g_{i_g} \cdot W_{i_g} + g_{\text{bal}_g} \cdot W_{\text{bal}_g} \tag{19}$$

where each W_x represents the WF of the corresponding partial cost function g_x. The GSC switching state that minimizes G_g is applied at the next sampling instant $(k+1)$. Due to space restrictions, switching frequency limitation is overlooked in this paper. The grid current vector error is minimized using the partial cost function

$$g_{i_g} = \left|\overline{\Delta i}\right| = \sqrt{\left(\Delta i^p_{g_\alpha}\left[k+2\right]\right)^2 + \left(\Delta i^p_{g_\beta}\left[k+2\right]\right)^2} \tag{20}$$

where the current error components are given by (27)[1] shown at bottom of the next page. The grid current references ($i^*_{g_\alpha}$ and $i^*_{g_\beta}$) are synchronized with the grid voltage using a PLL (for unity power factor) and their amplitude is calculated using a PI controller with the dc bus voltage error as input and the reference power as output.

The dc bus capacitor voltage unbalance at $k+2$ can be calculated using (28) shown at bottom of the next page. However, this expression requires all converters to be considered simultaneously, which would critically increase the required amount of calculations (discussed in Section V). For this reason, each converter is considered as an independent MPC system. Hence, the GSC considers only its own impact on the capacitor voltage balance [only γ_{bal_g} is considered in (28)], resulting in the partial cost function

$$g_{\text{bal}_g} = \left|\Delta v^p_C\left[k+1\right] - \frac{T_s}{C_{\text{dc}}} i_{M_g}\left[k+1\right]\right|. \tag{21}$$

[1]Note: the corresponding β component is obtained analogously.

B. Load-Side Controller

The global load-side controller cost function is given by

$$G_L = g_v \cdot W_v + g_{i_L} + g_{\mathrm{bal}_L} \cdot W_{\mathrm{bal}_L} \tag{22}$$

and includes three objectives: minimization of the load voltage vector error (g_v); limitation of the LSC current (g_{i_L}); and the balancing of the dc bus capacitors (g_{bal_L}).

The load voltage error is minimized using the cost function

$$g_v = \sqrt{\left(\Delta v^p_{\mathrm{load}_\alpha}[k+2]\right)^2 + \left(\Delta v^p_{\mathrm{load}_\beta}[k+2]\right)^2} \tag{23}$$

where the load voltage error is given by (29)[2] shown at bottom of this page. The load voltage references are sinusoidal three-phase signals with the desired UPS output voltage frequency and amplitude. The LSC currents at $k+2$, given by (30)[2] shown at bottom of this page, are limited to $I_{L_{\max}}$ using the constraint

$$g_{i_L} = \begin{cases} 0\,, & \left|\bar{i}^p_L[k+2]\right| \le I_{L_{\max}} \\ \infty\,, & \left|\bar{i}^p_L[k+2]\right| > I_{L_{\max}} \end{cases}. \tag{24}$$

The capacitor voltage balancing partial cost function is

$$g_{\mathrm{bal}_L} = \left|\Delta v^p_C[k+1] + \frac{T_s}{C_{\mathrm{dc}}} i_{M_L}[k+1]\right|. \tag{25}$$

C. DC–DC Controller

The global dc–dc controller cost function is given by

$$G_D = g_{i_{\mathrm{bat}}} \cdot W_{i_{\mathrm{bat}}} + g_{\mathrm{bal}_D} \cdot W_{\mathrm{bal}_D} \tag{26}$$

and includes two objectives: minimization of battery current error ($g_{i_{\mathrm{bat}}}$); and the balancing of the dc bus capacitors (g_{bal_D}). The battery current error is minimized by the partial cost function

$$g_i = \left|\Delta i_{\mathrm{bat}}[k+2]\right| \tag{32}$$

[2]Note: the corresponding β component is obtained analogously.

where $\Delta i_{\mathrm{bat}}[k+2]$ is obtained using (31) shown at bottom of this page. The capacitor voltage balancing partial cost function is defined as

$$g_{\mathrm{bal}_L} = \left|\Delta v^p_C[k+1] + \frac{T_s}{C_{\mathrm{dc}}} i_{M_L}[k+1]\right|. \tag{33}$$

In normal operation (energy flowing from the grid), the batteries are charged (when needed) at an optimal current level, dictated by a battery management system. In stored energy mode, the batteries are discharged in order to keep the dc bus stable. In this case, the battery current reference i^*_{bat} is calculated using the same PI controller used for the GSC.

D. WF Selection

Since there is no analytical method to determine the optimal OSV-MPC WFs, they are selected through extensive simulation and testing. More importantly, the same WFs do not provide optimal performance at all operating points [8]–[10]. For example, WFs selected for optimal performance at full-load do not ensure appropriate capacitor balance in a no-load condition (shown in Section VII). Hence, WFs must be selected to ensure *acceptable* operation in all conditions, sacrificing performance in the most common cases (e.g., full-load).

WFs are selected according to the performance objectives described as follows by order of priority:

1) Minimize $\mathrm{THD}_{v_{\mathrm{load}}}$.
2) Minimize THD_{i_g}.
3) Keep $|\Delta v_C|_{\max} < 0.05\, v^*_{\mathrm{dc}}$ in steady-state.
4) Minimize $\Delta v_{C_{\mathrm{RMS}}}$.

V. Cooperative OSV-MPC Controllers

The controllers shown in the previous section consider each converter as an independent system, overlooking the effect of each other on the dc bus. This leads to a nonoptimal control action. An optimal solution would be to use a single, unified, OSV-MPC controller for the whole UPS. However, this would require the full model of the UPS to be computed

$$\Delta i^p_{g_\alpha}[k+2] = \underbrace{i^*_{g_\alpha}[k+2] - \left(1 - \frac{R_g T_s}{L_g}\right) i^p_{g_\alpha}[k+1] - \frac{T_s}{L_g} v^p_{s_\alpha}[k+1]}_{\varphi_{i_{g_\alpha}}\ \text{(fixed)}} + \underbrace{\frac{T_s}{L} v_{g_\alpha}[k+1]}_{\gamma_{i_{g_\alpha}}\ \text{(variable)}} \tag{27}$$

$$\Delta v^p_C[k+2] = \underbrace{v^p_{C_1}[k+1] - v^p_{C_2}[k+1]}_{\varphi_{\mathrm{bal}}\ \text{(fixed)}} + \underbrace{\left(-\frac{T_s}{C_{\mathrm{dc}}} i_{M_g}[k+1]\right)}_{\gamma_{\mathrm{bal}_g}\ \text{(variable)}} + \underbrace{\frac{T_s}{C_{\mathrm{dc}}} i_{M_L}[k+1]}_{\gamma_{\mathrm{bal}_L}\ \text{(variable)}} + \underbrace{\frac{T_s}{C_{\mathrm{dc}}} i_{M_D}[k+1]}_{\gamma_{\mathrm{bal}_D}\ \text{(variable)}} \tag{28}$$

$$\Delta v^p_{\mathrm{load}_\alpha}[k+2] = \underbrace{v^*_{\mathrm{load}_\alpha}[k+2] - A_{21} i^p_{L_\alpha}[k+1] - A_{22} v^p_{\mathrm{load}_\alpha}[k+1] - A_{23} \hat{i}_{\mathrm{load}_\alpha}[k+1]}_{\varphi_{v_\alpha}\ \text{(fixed)}} + \underbrace{(-B_2 v_{L_\alpha}[k+1])}_{\gamma_{v_\alpha}\ \text{(variable)}} \tag{29}$$

$$i^p_{L_\alpha}[k+2] = A_{11} i^p_{L_\alpha}[k+1] + A_{12} v^p_{\mathrm{load}_\alpha}[k+1] + A_{13} \hat{i}_{\mathrm{load}_\alpha}[k+1] + B_1 v_{L_\alpha}[k+1] \tag{30}$$

$$\Delta i^p_{\mathrm{bat}}[k+2] = \underbrace{i^*_{\mathrm{bat}}[k+2] - i^p_{\mathrm{bat}}[k+1] + \frac{R_D T_S}{L_D} i^p_{\mathrm{bat}}[k+1] + \frac{T_S}{L_D} v^p_{\mathrm{bat}}[k+1]}_{\varphi_{i_{\mathrm{bat}}}\ \text{(fixed)}} + \underbrace{\left(-\frac{T_S}{L_D} v_D[k+1]\right)}_{\gamma_{i_{\mathrm{bat}}}\ \text{(variable)}} \tag{31}$$

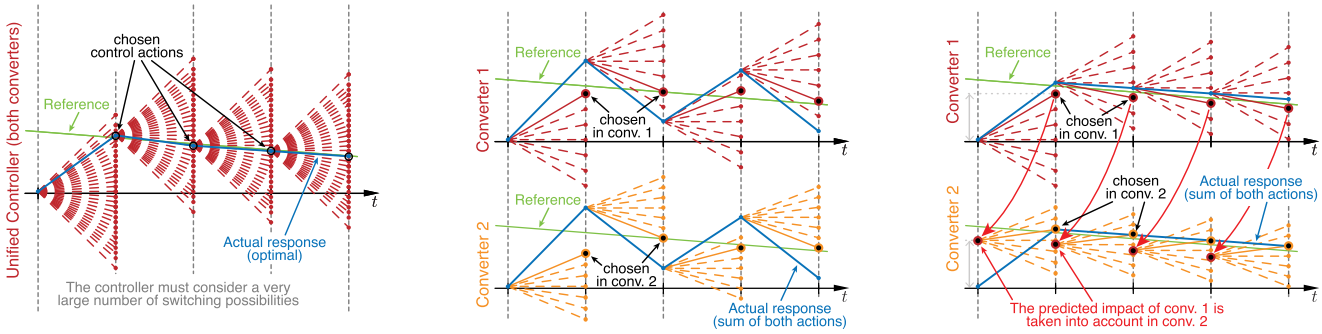

Fig. 3. Illustrative representation of the response obtained with two converters controlling a common variable, with different control approaches. (a) Unified controller. (b) Independent controllers. (c) Proposed cooperative controllers.

$27 \times 27 \times 4 = 2916$ times. In comparison, the independent solution requires the model of each 3LNPC converter to be computed only 27 times and the 3LDC converter four times. Hence, due to its incredibly steep computational cost, a unified controller is typically unfeasible in industrial solutions, justifying the common use of independent controllers.

An illustrative comparison of the unified and independent controllers response is shown in Fig. 3(a) and (b), for the case of two converters controlling a common variable. As illustrated in Fig. 3(b), even though each independent controller attempts to minimize the error on the common variable, their combined action produces a nonoptimal response (in blue). In the UPS, this means a higher capacitor voltage unbalance (oscillation). In addition, this can lead to a deterioration of the remaining waveforms, since a higher error in one objective is more likely to lead to nonoptimal action on the others—leading to a lower overall performance.

A new approach is now proposed to minimize the drawbacks of independent controllers, with the same computational cost. This technique is denoted as cooperative OSV-MPC (Co-MPC) and proposes that one of the converters is made aware of the action of the other, in order to complement it. This way, instead of both controllers making a "blind" choice (overlooking the other converter), the second converter takes the predicted impact of the action already selected by the first one into account. This principle is illustrated in Fig. 3(c). As shown, by taking the action of the first converter into account, the second controller can effectively predict the actual response of the system and therefore select an optimal action regarding the common objective. This significantly improves the combined response of the two converters when compared to fully independent controllers [compare Fig. 3(b) and (c)].

Since the second controller can correct (or degrade) the action of the first one, it inherently has a higher responsibility regarding the common objective—a hierarchy is created. In a UPS system, the main priority is to supply a high-quality load voltage waveform. Hence, the LSC gives a low importance to the capacitor balancing and is more likely to have a negative impact on it. Thus, the LSC controller is computed first. Then, the DCC controller is computed, taking the impact of the selected LSC action (γ_{bal_L}) into account. Finally, the GSC is computed, taking the impact of both the LSC and DCC (γ_{bal_L} and γ_{bal_D}) into account (shown in Fig. 2) and thus accurately predicting the dc bus state at $k+2$. Hence, the GSC has the highest responsibility in maintaining capacitor balance.

This technique requires practically the same amount of calculations as independent controllers, so it effectively improves system performance without reducing its practical feasibility. Besides improving control over the common objective, the definition of a hierarchy also allows the system to improve the remaining objectives. This approach can be used in any system with multiple converters. Co-MPC improves the steady-state performance of the system, but has little impact on the transient response. However, it can be perfectly combined with the dynamic behavior of DWMPC.

VI. Cooperative Dynamically Weighted MPC

DWMPC, proposed in [10], uses a new cost function formulation and dynamically adjusts WF in real-time to achieve a highly adaptable behavior. This improves both steady-state performance and dynamic response. The results presented in [10] demonstrate the excellent performance of DWMPC when applied to a single converter (a 3LNPC rectifier), but its potential advantages when applied to multiconverter systems were never discussed. This paper proposes new DWMPC controllers for all converters of the 3-level UPS system, combined with the new cooperative principle. The proposed cooperative DWMPC (Co-DWMPC) controllers take advantage of both the dynamic nature of DWMPC and the improved cooperation of Co-MPC, improving both the steady-state performance and the dynamic response.

DWMPC is based on the analysis of the fixed and variable components of the conventional OSV-MPC cost functions [denoted as φ_x and γ_x in expressions (27)–(31)].

The DWMPC partial cost function is generically defined as

$$\hat{g}_x = \frac{\lceil \varphi_x \rceil + \gamma_x}{2\gamma_{x_{\max}}} \tag{34}$$

$$\lceil \varphi_x \rceil = \begin{cases} \varphi_x \ , & |\varphi_x| \le \gamma_{x_{\max}} \\ \gamma_{x_{\max}} \cdot \operatorname{sign}(\varphi_x) \ , & |\varphi_x| > \gamma_{x_{\max}} \end{cases} \tag{35}$$

where $\gamma_{x_{\max}}$ represents the maximum value that the variable term γ_x can take for the available control set.

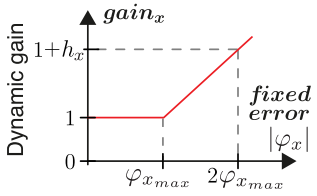

Fig. 4. Dynamic gain profile for objective x.

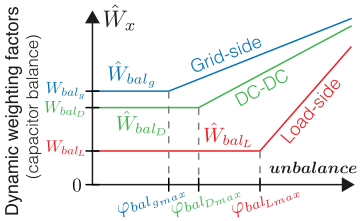

Fig. 5. Dynamic WF of the three UPS converters for dc bus balancing.

The dynamic WFs in DWMPC are defined as

$$\hat{W}_x = \text{gain}_x \cdot W_x \tag{36}$$

where W_x is the constant weight of objective x and gain_x represents the respective dynamic gain, given by

$$\text{gain}_x = \begin{cases} 1\,, & |\varphi_x| \le \varphi_{x_{\max}} \\ |\varphi_x| \frac{h_x}{\varphi_{x_{\max}}} + (1 - h_x)\,, & |\varphi_x| > \varphi_{x_{\max}} \end{cases} \tag{37}$$

where $\varphi_{x_{\max}}$ represents the maximum error considered admissible in steady-state and h_x a chosen weight increase rate. This results in the gain profile shown in Fig. 4. As visible in this figure, $\text{gain}_x = 1$ as long as the fixed error component φ_x (independent from the converter action) remains below the maximum limit $\varphi_{x_{\max}}$. In these conditions, the WF is constant ($\hat{W}_x = W_x$), operating similarly to the conventional OSV-MPC. However, when φ_x surpasses $\varphi_{x_{\max}}$, the dynamic gain and, consequently, the WF, increases with the error (linearly). This gives a higher priority to the correction of large errors.

Besides improving the response of a single converter, this dynamic behavior is extremely useful when applied to multi-converter systems, such as the proposed UPS. As described, the main objective of the LSC is to supply a high-quality load voltage waveform. This way, a low dc balancing weight is typically chosen for the LSC (W_{bal_L}), to improve the load voltage. However, a low W_{bal_L} also means that the LSC has a very low contribution to eliminate existing unbalances. Since a large unbalance can compromise the operation of the system, all converters should contribute significantly to correct it, but this would be impossible with the same W_{bal_L}. On the other hand, the dynamic WFs of DWMPC can present a low value in steady-state and increase when the error rises.

This paper proposes the use of DWMPC on all UPS converters, with WF profiles as illustrated in Fig. 5. As shown, when the capacitors are balanced (approximately) the LSC has a very low $\hat{W}_{\text{bal}_L}$, focusing mostly on improving the load voltage waveform. In these conditions, the other converters have significantly higher weights, but still low enough to ensure low current distortion in steady-state. If the existing unbalance surpasses $\varphi_{\text{bal}_{g\max}}$ and $\varphi_{\text{bal}_{D\max}}$, the WFs of the GSC and DCC start to increase, in order to correct it. If these two converters cannot correct the unbalance and it surpasses $\varphi_{\text{bal}_{L\max}}$, the LSC will provide assistance in correcting it. Above this limit, $\hat{W}_{\text{bal}_L}$ is also increased as a function of the error. This may temporarily decrease the load voltage waveform quality, but guarantees a fast error correction, allowing steady-state to be restored. This perfectly complements the hierarchy defined by the cooperative technique.

Moreover, DWMPC can adapt to different operating points, leading to higher overall performance in distinct conditions. Hence, Co-DWMPC ensures very high steady-state performance and improved dynamic response.

The proposed Co-DWMPC controllers are presented next. The dynamic WFs are obtained, at each sampling instant, using (36) and (37), where φ_x is obtained from (27)–(31).

A. Load-Side Controller

The global load-side cost function is given by

$$\hat{G}_L = \hat{g}_v \cdot \hat{W}_v + \hat{g}_{\text{bal}_L} \cdot \hat{W}_{\text{bal}_L} + g_{i_L}\,. \tag{38}$$

The partial cost function regarding the load voltage is

$$\hat{g}_v = \frac{|\lceil \overline{\varphi}_v \rceil + \overline{\gamma}_v|}{2\gamma_{v_{\max}}} = \frac{\sqrt{\left(\lceil \varphi_{v_\alpha} \rceil + \gamma_{v_\alpha}\right)^2 + \left(\lceil \varphi_{v_\beta} \rceil + \gamma_{v_\beta}\right)^2}}{2 \cdot \frac{2}{3} B_2 v_{\text{dc}}} \tag{39}$$

Given that this function concerns a vector instead of a scalar value, the limited fixed vector $\lceil \overline{\varphi}_v \rceil$ is not obtained from (35), but using the following mathematical manipulation [10]

$$m + jn = \frac{\varphi_{v_\alpha} + j\varphi_{v_\beta}}{\gamma_{v_{\max}}} \cdot e^{j\theta} \tag{40}$$

$$\lceil m \rceil = \begin{cases} m, & m \le \frac{\sqrt{3}}{2} \\ \frac{\sqrt{3}}{2}, & m > \frac{\sqrt{3}}{2} \end{cases}; \quad \lceil n \rceil = \begin{cases} n, & |n| \le \frac{1}{2} \\ \frac{1}{2} \cdot \text{sign}\,(n)\,, & |n| > \frac{1}{2} \end{cases} \tag{41}$$

$$\lceil \overline{\varphi}_v \rceil = \lceil \varphi_{v_\alpha} \rceil + j \lceil \varphi_{v_\beta} \rceil = \gamma_{v_{\max}} \left(\lceil m \rceil + j \lceil n \rceil \right) \cdot e^{-j\theta} \tag{42}$$

where $\theta = \left(\frac{\pi}{6} - \frac{\pi}{3} \cdot \text{Sector}\right)$ and Sector represents the sector in which the fixed vector $\overline{\varphi}_v$ is located [10].

As defined by the cooperative principle, the LSC overlooks the impact of the other converters on the dc bus [$\varphi_{\text{bal}_L} = \varphi_{\text{bal}}$, from (28)]. The capacitor voltage balancing cost function is

$$\hat{g}_{\text{bal}_L} = \frac{\lceil \varphi_{\text{bal}_L} \rceil + \gamma_{\text{bal}_L}}{2 \cdot \frac{T_s}{C_{\text{dc}}} \cdot \max\left(|i_A|, |i_B|, |i_C|\right)} \tag{43}$$

where $\lceil \varphi_{\text{bal}_L} \rceil$ is obtained from (35).

B. DC–DC Controller

The global dc–dc cost function is given by

$$\hat{G}_D = \hat{g}_{i_{\text{bat}}} \cdot \hat{W}_{i_{\text{bat}}} + \hat{g}_{\text{bal}_D} \cdot \hat{W}_{\text{bal}_D}\,. \tag{44}$$

The battery current partial cost function is defined as

$$\hat{g}_{i_{\text{bat}}} = \frac{\lceil \varphi_{i_{\text{bat}}} \rceil + \gamma_{i_{\text{bat}}}}{2 \cdot \frac{T_s}{L_D} v_{\text{dc}}}\,. \tag{45}$$

TABLE I
SELECTED DWMPC PARAMETERS AND EFFECTS OF PARAMETER CHANGE

	Controller Parameter	Selected Value	System Effect	Effect of parameter increase (↑)	Effect of parameter decrease (↓)
GSC	W_{bal_g} [1]	0.01	***SS+T***	$\text{THD}_{i_g}\nearrow$ & $\lvert\Delta v_C\rvert\searrow$	$\text{THD}_{i_g}\searrow$ & $\lvert\Delta v_C\rvert\nearrow$ [2]
	$\varphi_{i_{g_{max}}}$	0.3 A	***SS***	increase of acceptable $\lvert\Delta\bar{i}_g\rvert \Rightarrow \text{THD}_{i_g}\nearrow$ & $\lvert\Delta v_C\rvert\searrow$	$\text{THD}_{i_g}\searrow$ & $\lvert\Delta v_C\rvert\nearrow$ [2] ; lower values may lead to chattering
	$\varphi_{bal_{g_{max}}}$	1 V	***SS***	$\text{THD}_{i_g}\searrow$ & $\lvert\Delta v_C\rvert\nearrow$ [2]	$\text{THD}_{i_g}\nearrow$ & $\lvert\Delta v_C\rvert\searrow$
	h_{i_g}	1	***T***	faster correction of large $\Delta\bar{i}_g$ & higher $\lvert\Delta v_C\rvert$ during transients	slower $\bar{i}_g$ tracking & lower $\lvert\Delta v_C\rvert$ during transients
	h_{bal_g}	10	***T***	faster correction of large Δv_C & worse $\bar{i}_g$ tracking	slower correction of large Δv_C [2] & better $\bar{i}_g$ tracking
DCC	W_{bal_D} [1]	0.01	***SS+T***	$\lvert\Delta i_{bat}\rvert\nearrow$ & $\lvert\Delta v_C\rvert\searrow$	$\lvert\Delta i_{bat}\rvert\searrow$ & $\lvert\Delta v_C\rvert\nearrow$ [2]
	$\varphi_{i_{bat_{max}}}$	0.3 A	***SS***	$\lvert\Delta i_{bat}\rvert\nearrow$ & $\lvert\Delta v_C\rvert\searrow$	$\lvert\Delta i_{bat}\rvert\searrow$ & $\lvert\Delta v_C\rvert\nearrow$ [2]
	$\varphi_{bal_{D_{max}}}$	1 V	***SS***	$\lvert\Delta i_{bat}\rvert\searrow$ & $\lvert\Delta v_C\rvert\nearrow$ [2]	$\lvert\Delta i_{bat}\rvert\nearrow$ & $\lvert\Delta v_C\rvert\searrow$
	$h_{i_{bat}}$	1	***T***	faster correction of large Δi_{bat} & higher $\lvert\Delta v_C\rvert$ during transients	slower i_{bat} tracking & lower $\lvert\Delta v_C\rvert$ during transients
	h_{bal_D}	10	***T***	faster correction of large Δv_C & worse i_{bat} tracking	slower correction of large Δv_C [2] & better i_{bat} tracking
LSC	W_{bal_L} [1]	0.001	***SS+T***	$\text{THD}_{v_{load}}\nearrow$ & $\lvert\Delta v_C\rvert\searrow$	$\text{THD}_{v_{load}}\searrow$ & $\lvert\Delta v_C\rvert\nearrow$
	$\varphi_{v_{max}}$	1 V	***SS***	increase of acceptable $\lvert\Delta\bar{v}_{load}\rvert \Rightarrow \text{THD}_{v_{load}}\nearrow$ & $\lvert\Delta v_C\rvert\searrow$	$\text{THD}_{v_{load}}\searrow$ & $\lvert\Delta v_C\rvert\nearrow$; lower values may lead to chattering
	$\varphi_{bal_{L_{max}}}$	10 V	***SS+T***	LSC only helps correct large $\Delta v_C \Rightarrow \lvert\Delta v_C\rvert_{\boldsymbol{T}}\nearrow$ & $\lvert\Delta\bar{v}_{load}\rvert_{\boldsymbol{T}}\searrow$	LSC helps correct smaller $\Delta v_C \Rightarrow \lvert\Delta v_C\rvert_{\boldsymbol{SS+T}}\searrow$ & $\text{THD}_{v_{load}}\nearrow$
	h_v	1	***T***	faster correction of large $\Delta\bar{v}_{load}$ & higher $\lvert\Delta v_C\rvert$ during transients	slower $\bar{v}_{load}$ tracking & lower $\lvert\Delta v_C\rvert$ during transients
	h_{bal_L}	20	***T***	faster correction of large Δv_C & higher transient $\lvert\Delta\bar{v}_{load}\rvert$	slower correction of large Δv_C & lower transient $\lvert\Delta\bar{v}_{load}\rvert$

[1] For design simplicity, constant weights W_{i_g}, $W_{i_{\text{bat}}}$, and W_v are left constant (= 1) and only their complementary weights are adjusted.
[2] If the capacitor unbalance $\lvert\Delta v_C\rvert$ increases significantly, this may impact $\text{THD}_{v_{\text{load}}}$.
Note: The described effect of each parameter change merely displays the general trend, it is not universally valid (increasing a given weight indefinitely does not produce the lowest possible respective error [8], [9]); (*SS* = steady-state; *T* = transients; ↗ = tends to increase; ↘ = tends to decrease).

As per the Co-MPC principle, this converter takes into account the action already selected by the LSC. Thus, the fixed error component φ_{bal_D} now includes the predicted effect of the action selected for LSC (γ_{bal_L}): $\varphi_{\text{bal}_D} = \varphi_{\text{bal}} + \gamma_{\text{bal}_L}$. The capacitor balancing cost function is given by

$$\hat{g}_{\text{bal}_D} = \frac{\lceil\varphi_{\text{bal}_D}\rceil + \gamma_{\text{bal}_D}}{2\cdot\frac{T_s}{C_{\text{dc}}}\cdot\lvert i_{\text{bat}}\rvert}\ . \tag{46}$$

C. Grid-Side Controller

The global grid-side cost function is

$$\hat{G}_g = \hat{g}_{i_g}\cdot\hat{W}_{i_g} + \hat{g}_{\text{bal}_g}\cdot\hat{W}_{\text{bal}_g}\ . \tag{47}$$

The grid current cost function is defined as

$$\hat{g}_{i_g} = \frac{\left|\lceil\overline{\varphi}_{i_g}\rceil + \overline{\gamma_{i_g}}\right|}{2\gamma_{i_{g\max}}} = \frac{\sqrt{\left(\lceil\varphi_{i_{g\alpha}}\rceil+\gamma_{i_{g\alpha}}\right)^2+\left(\lceil\varphi_{i_{g\beta}}\rceil+\gamma_{i_{g\beta}}\right)^2}}{2\cdot\frac{2}{3}\frac{T_s}{L_g}v_{dc}} \tag{48}$$

where the limited fixed vector $\lceil\overline{\varphi}_{i_g}\rceil$ is obtained in a similar manner to what is shown in (40)–(42) and in [10].

Regarding the dc bus capacitor voltage balancing, the GSC considers the influence of all converters. For this reason, the fixed error component is now $\varphi_{\text{bal}_g} = \varphi_{\text{bal}} + \gamma_{\text{bal}_L} + \gamma_{\text{bal}_D}$. Hence, the capacitor voltage balancing cost function is

$$\hat{g}_{\text{bal}_g} = \frac{\lceil\varphi_{\text{bal}_g}\rceil + \gamma_{\text{bal}_g}}{2\cdot\frac{T_s}{C_{\text{dc}}}\cdot\max\left(\lvert i_R\rvert,\lvert i_S\rvert,\lvert i_T\rvert\right)}\ . \tag{49}$$

D. DWMPC Parameter Selection

As with the conventional OSV-MPC, there is no analytical method to select optimal controller parameters, so these must also be selected through testing. Even though DWMPC has more parameters than the conventional OSV-MPC, parameter fine-tuning is not as critical, due to its dynamic behavior.

A suggested controller design procedure is now described as follows.

First, the LSC and GSC controllers are tuned. Start with all parameters set to one, but all $\varphi_{x_{\max}} = \infty$. For full load, adjust the constant weights W_x until optimal results are obtained (according to the criteria in Section IV-D)—this adjusts the constant region of the controller. Then, choose the maximum errors $\varphi_{x_{\max}}$ close to the error levels seen with the chosen W_x at full-load. $\varphi_{\text{bal}_{L\max}}$ is set to a higher value, to ensure that the LSC does not affect the load voltage waveform unless that unbalance value is surpassed (during transients). Next, adjust h_x to ensure adequate controller adaptation to different steady-state conditions: at no-load, adjust h_{bal_g} to ensure that the GSC can keep the capacitor unbalance within the chosen limits (with no load, the UPS has minimum balancing capability). Since only two concurrent objectives are used in each converter, W_x and h_x are adjusted only for the capacitor balancing and kept equal to one in the remaining objectives, for design simplicity. Next, cause a large error in each objective (e.g., quickly discharge one of the capacitors to cause a large unbalance or cause a large load step) and adjust h_x to ensure a fast error correction, with acceptable impact on the remaining objectives. For example, increasing h_{bal_L} ensures the LSC contributes more significantly to correct large unbalances, but leads to a higher v_{load} error until the unbalance is corrected. This adjusts the dynamic region of the controller. Finally, test the controller in different steady-state conditions and with different transients to fine-tune the design. Last, repeat the process for stored energy mode (DCC and LSC) and with all converters, to adjust the parameters of the DCC (only).

The parameters selected for each controller are shown in Table I, as well as the main effects of changing each of them.

VII. EXPERIMENTAL RESULTS

Experimental results are now presented, demonstrating the advantages of each proposed control technique. A fully functional prototype of the proposed UPS system was developed, as shown in Fig. 6. All circuit and controller parameters are shown in Table II. For prototype safety, the grid voltage is adjusted to 120 V (rms) with an autotransformer. A linear and a highly nonlinear load are used (described in Table II). All controllers are

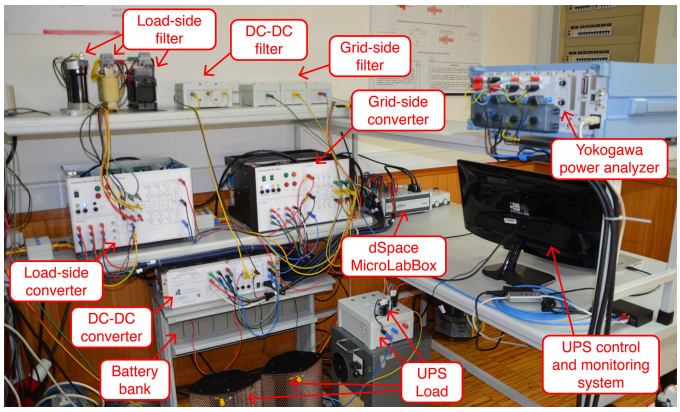

Fig. 6. Experimental prototype of the proposed UPS system.

TABLE II
EXPERIMENTAL CIRCUIT AND CONTROL PARAMETERS

Circuit Parameters	Values	Controller Parameter	Value
GSC filter (L_g, R_g)	13.5 mH, 0.2 Ω	Sampling time (T_s)	70 μs
LSC filter (L_L, R_L, C_L)	2.7 mH, 0.1 Ω, 66 mF	DC bus voltage ref. (v^*_{DC})	220 V
DCC filter (L_D, R_D)	14 mH, 0.3 Ω	Load voltage ref. (rms)	120 V
DC bus cap. (C_{DC})	208 μF	Max. grid current ref.	15 A
Battery voltage (V_{bat})	10 × 12 V (lead-acid)	Max. battery current ref.	10 A
Supply voltage (V_s)	120 V (rms)	Max. LSC current ($I_{L_{max}}$)	15 A
Non-linear load	3∼ rect. → 35 Ω // 180 μF	Charge horizon (N_{charge})	80
Linear load	Δ-connected 50 Ω	Max. cap. voltage ($v_{C_{max}}$)	130 V

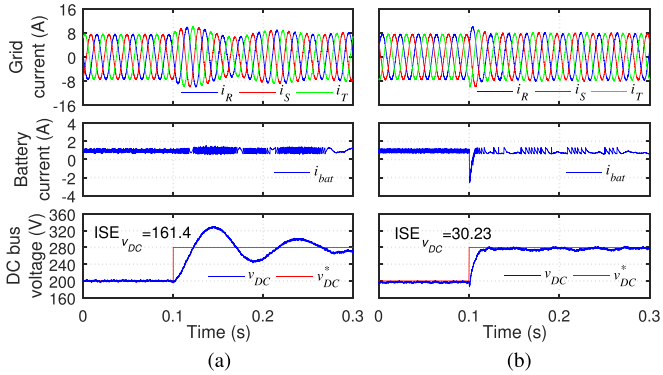

Fig. 7. UPS response during dc bus voltage reference step. (a) PI controller. (b) Proposed PMS.

implemented in *MATLAB/Simulink* and executed in real-time in a *dSpace MicroLabBox*. The proposed controller displays only slightly higher execution time than the conventional case (47.0 μs versus 44.6 μs). A Yokogawa WT3000 power analyzer is used to monitor system performance.

A. Power Management System

Fig. 7 demonstrates the UPS response when the dc bus voltage reference is changed from 200 to 280 V, with the conventional PI-based controller and the proposed PMS. In this test, the LSC feeds a linear load (described in Table II) and the DCC charges the batteries with a current of 1 A. For a fair comparison, the proposed Co-DWMPC controllers are used in both cases, only the PMS differs. As shown by these results, the PI-based solution presents significant overshoot and oscillations after the reference

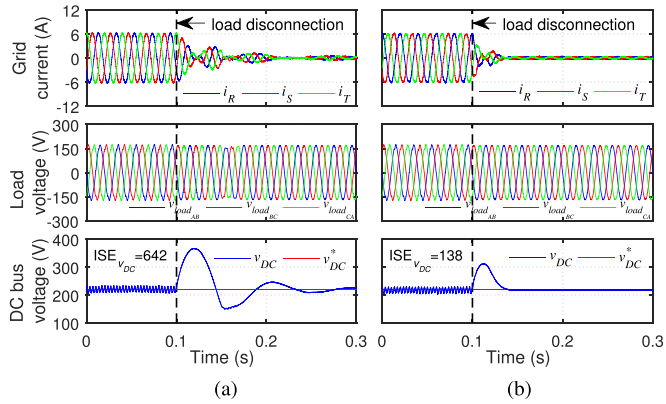

Fig. 8. UPS response during load step (nonlinear load disconnection). (a) PI controller. (b) Proposed PMS.

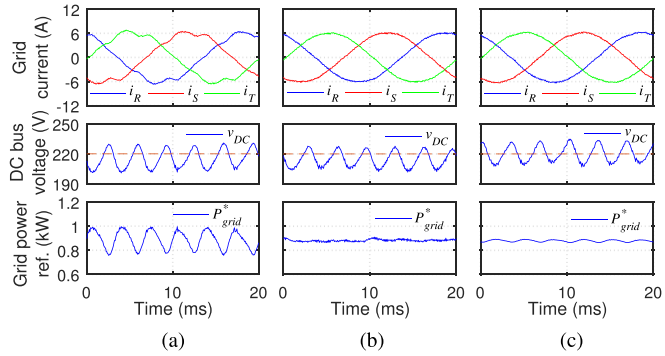

Fig. 9. Steady-state grid current when feeding a nonlinear load. (a) PMS w/out $\tilde{p}_L$ comp. (b) PMS w/ $\tilde{p}_L$ comp. (c) PI controller.

step. On the other hand, the proposed controller provides very fast dc bus voltage adjustment, with no overshoot. The integral squared error (ISE) of $v_{\rm dc}$ for both cases (calculated for the displayed time window) reflects the improved voltage regulation of the proposed PMS. With the proposed PMS the DCC also aids in charging the dc bus, drawing current from the batteries during the transient, as visible in Fig. 7(b). This helps speed up the voltage adjustment.

Fig. 8 demonstrates the UPS response during a load step (disconnection of a nonlinear load). Only the PMS differs in the control system. As shown in the figure, the sudden load disconnection leads to a transient dc bus voltage increase, which must be corrected by the controller. Comparing Fig. 8(a) and (b), it is clear that the proposed PMS provides faster voltage regulation than the PI-based solution, with no overshoot and no oscillatory behavior. This produces a significantly lower $\text{ISE}_{v_{\rm dc}}$, as shown in the figure.

Fig. 9 shows the grid current and grid power reference in steady-state, when feeding a nonlinear load. As shown in Fig. 9(a), when $P^*_{\rm charge}$ is calculated without the proposed $\tilde{p_L}$ compensation (16) the dc bus voltage oscillation is reflected in $P^*_{\rm grid}$, leading to considerable grid current distortion. On the other hand, when $\tilde{p_L}$ is considered near sinusoidal grid currents are obtained. Fig. 9 also demonstrates the main disadvantage of the proposed PMS – $v_{\rm dc}$ presents a steady-state error. However,

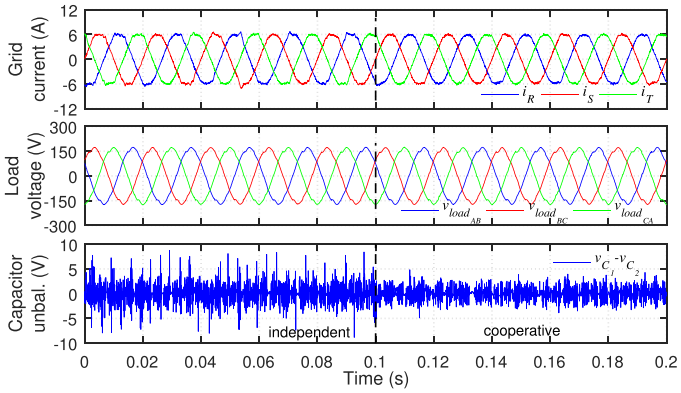

Fig. 10. UPS operation with independent and cooperative controllers.

TABLE III
SELECTED MPC CONTROLLER PARAMETERS

Case	Description	W_{bal_g}	W_{bal_L}	W_{bal_D}
MPC (optimal)	WFs selected through extensive testing for proper operation *in all operating points* (*used*)	0.3	0.01	0.3
MPC (nonoptimal)	Non-optimal WFs, selected *only* for optimized performance with nonlinear load (*illustrative*)	0.01	0.001	0.01

Note: For design simplicity, W_{i_g}, $W_{i_{\mathrm{bat}}}$, and W_v are left constant ($=1$) and only their complementary weights are adjusted.

this small mean value deviation (≈4.8 V) has no tangible impact on the UPS operation.

As shown in Fig. 9(c), the PI-based controller also produces a slight P^*_{grid} oscillation. This is due to the proportional component of the PI and represents a major challenge in the design of the PI controller. The proportional term is important to obtain a faster response and/or lower overshoot, but it also compromises steady-state grid current distortion, making the PI design very difficult. On the other hand, the proposed solution requires very little design effort.

B. Cooperative Control Principle

The advantages of the proposed cooperative principle are demonstrated in Fig. 10. This figure displays the steady-state behavior of the UPS when feeding a nonlinear load, with the conventional OSV-MPC controllers. The controllers are changed from fully independent to cooperative at $t = 0.1$ s (only the cooperative technique varies during this test). When the cooperative principle is used, the capacitor balance is clearly improved. In addition, performance is improved on the remaining waveforms (especially the grid current). This is clearly shown in Table IV (compare case ① with ④, and ③ with ⑤). With the conventional OSV-MPC, for example, using the cooperative principle reduces $|\Delta v_C|_{\max}$ from 15.3 to 9.9 V and THD_{i_g} from 3.5 to 2.6%.

C. DWMPC Controllers

In order to demonstrate the advantages of the proposed DWMPC controllers, the shortcomings of the conventional OSV-MPC are first demonstrated. After extensive testing, and

TABLE IV
UPS POWER QUALITY WITH OSV-MPC AND DWMPC

Case	Controller	THD_{i_g}	$\mathrm{THD}_{v_{load}}$	$\lvert\Delta v_C\rvert_{max}$	$\Delta v_{C_{RMS}}$	$\overline{f_{sw_g}}$	$\overline{f_{sw_L}}$
	UPS operation feeding a non-linear load (3∼ rect. $\rightarrow 35\,\Omega // 180\,\mu F$*)*						
①	Co-MPC (optimal)	**2.6%**	**3.4%**	**9.9 V**	2.5 V	4.0 kHz	5.0 kHz
②	Co-MPC (non-optimal)	0.9%	3.1%	10.8 V	2.3 V	3.7 kHz	4.9 kHz
③	Co-DWMPC	**0.9%**	**3.1%**	**7.4 V**	2.3 V	3.9 kHz	4.9 kHz
④	MPC (optimal)	**3.5%**	**3.4%**	**15.3 V**	3.1 V	4.2 kHz	5.1 kHz
⑤	DWMPC	1.3%	3.3%	11 V	2.5 V	4.0 kHz	4.9 kHz
	UPS operation at no-load						
①	Co-MPC (optimal)	8.4%	**0.35%**	**9.4 V**	**1.9 V**	3.1 kHz	5.1 kHz
②	Co-MPC (non-optimal)	10.7%	0.31%	**78.9 V**	**48.5 V**	2.6 kHz	4.2 kHz
③	Co-DWMPC	8.9%	**0.32%**	**6.2 V**	**1.0 V**	3.3 kHz	5.1 kHz
④	MPC (optimal)	8.8%	0.35%	11.2 V	2.8 V	3.2 kHz	5.2 kHz
⑤	DWMPC	10.1%	0.32%	9.4 V	3.3 V	3.2 kHz	5.2 kHz

Note: The proposed PMS is used in all cases. The UPS efficiency feeding the nonlinear load is slightly above 80% (a relatively low value, due to the low voltage and low load used for prototype safety).

according to the criteria described in Section IV-D, the weights identified as "optimal" in Table III have been selected for the OSV-MPC controllers. These WFs ensure *acceptable* performance *at all operating points*. However, to ensure adequate behavior in all conditions, performance cannot be optimized for each specific operating point. For example, the WFs identified as "nonoptimal" in Table III have been optimized *only* for operation with a nonlinear load and produce significantly lower current and voltage distortion than the optimal WFs with this load (compare cases ① and ② in Table IV). However, these WFs cannot maintain acceptable capacitor balance at no-load (reaching unbalance values as high as 78.9 V), and *cannot* be used in the controller. The WF selection must therefore compromise performance in each operating point to ensure *acceptable* performance in *all of them*.

Conversely, DWMPC controllers can adapt to different working conditions, optimizing performance in different points. As shown in Table IV, DWMPC can achieve excellent performance feeding the nonlinear load, while simultaneously ensuring very low capacitor unbalance at no-load (case ③). This way, when comparing the DWMPC solution with the conventional controller (with optimal weights), it is clear that it can provide better steady-state results at different load conditions (lower total harmonic distortion (THD) and lower unbalance).

The adaptability of the proposed DWMPC controllers is not only advantageous in steady-state, but also during transients and disturbances. Fig. 11 display the UPS response when a 3.2 Ω resistor is connected in parallel with capacitor C_2 for 1 ms, forcing its fast discharge. As visible in Fig. 11(a) and (b), the conventional OSV-MPC controller (with optimal WFs) can quickly correct the unbalance when supplying a load, but is unable to do the same at no-load (when the balancing capabilities of the UPS are low). At no-load, the system takes approximately 1.6 s to fully eliminate the capacitor unbalance. Fig. 11(b) also demonstrates that the proposed PMS effectively limits capacitor overvoltage during unbalances (v_{C1} is limited to $v_{C_{\max}} = 130$ V).

As shown in Fig. 11(c), when feeding a load, DWMPC ensures fast unbalance correction, with lower grid current and load voltage error than OSV-MPC (demonstrated by the lower ISE). On the other hand, when the balancing capabilities of the UPS

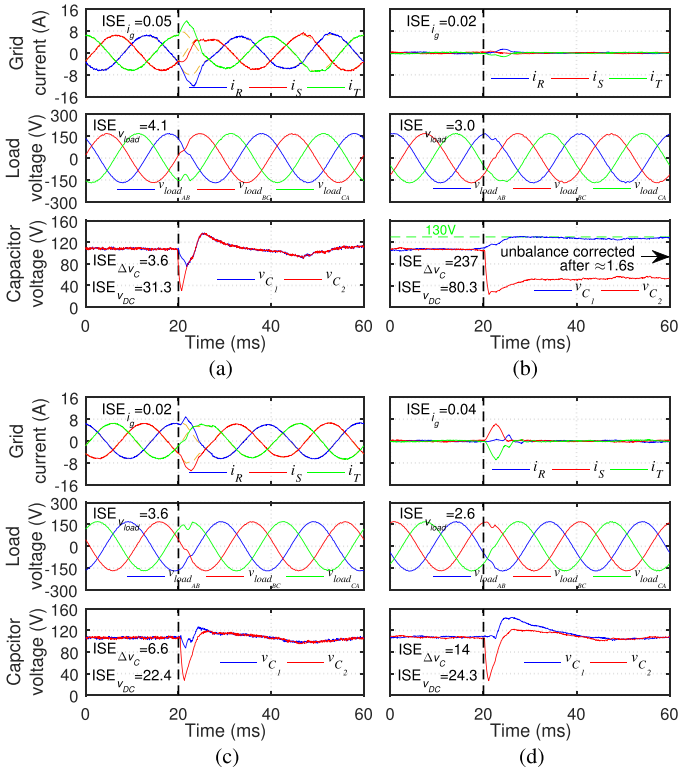

Fig. 11. UPS response during a forced discharge of capacitor C_2, with the proposed PMS and cooperative controllers: (a) OSV-MPC, feeding a linear load. (b) OSV-MPC, at no-load. (c) DWMPC, feeding a linear load. (d) DWMPC, at no-load.

are low (at no-load), DWMPC causes a higher grid current deviation (increase) in order to quickly correct the unbalance [visible in Fig. 11(d)]. Concurrently, the load voltage is less affected with DWMPC (lower ISE), since the LSC only contributes to correct the error while it is very large. This demonstrates the adaptability of the DWMPC controllers.

D. Overall System

The previous results demonstrate the advantages of each proposed novelty for the UPS control system. The overall system benefits from all these techniques are improved dynamic response, with faster error correction and no overshoot, and higher steady-state performance in different conditions, when compared to the conventional solutions.

VIII. Conclusion

In this paper, a 3-level uninterruptible power supply was proposed, using a new cooperative and dynamically weighted OSV-MPC controller. The proposed UPS system used multilevel converters in all stages, including the dc–dc. A new PMS was proposed, with very fast dynamic response and low design effort. A new cooperative control principle was proposed, improving multiconverter performance without increasing the overall computational cost. New controllers were proposed for all UPS converters, combining the new cooperative principle and the DWMPC technique.

The presented experimental results demonstrated the merits of each proposed novelty. The new PMS ensured very fast dc bus voltage tracking, with no overshoot, and low grid current distortion, even with highly nonlinear loads. The cooperative technique improved steady-state performance, leading to lower capacitor unbalance and waveform distortion than fully independent controllers. The DWMPC controllers provided great adaptability to different conditions, ensuring excellent steady-state performance under different loads (not possible with fixed WFs) and fast dynamic response and error correction, even in the presence of disturbances.

Hence, the proposed control system provided considerably better steady-state performance and dynamic response than the conventional OSV-MPC and PI-based solutions.

References

[1] H. Abu-Rub, S. Bayhan, S. Moinoddin, M. Malinowski, and J. Guzinski, "Medium-voltage drives: Challenges and existing technology," *IEEE Power Electron. Mag.*, vol. 3, no. 2, pp. 29–41, Jun. 2016.

[2] S. Vazquez, J. Rodriguez, M. Rivera, L. G. Franquelo, and M. Norambuena, "Model predictive control for power converters and drives: Advances and trends," *IEEE Trans. Ind. Electron.*, vol. 64, no. 2, pp. 935–947, Feb. 2017.

[3] A. Calle-Prado, S. Alepuz, J. Bordonau, P. Cortes, and J. Rodriguez, "Predictive control of a back-to-back NPC converter-based wind power system," *IEEE Trans. Ind. Electron.*, vol. 63, no. 7, pp. 4615–4627, Jul. 2016.

[4] Z. Zhang, C. M. Hackl, and R. Kennel, "Computationally efficient DMPC for three-level NPC back-to-back converters in wind turbine systems with PMSG," *IEEE Trans. Power Electron.*, vol. 32, no. 10, pp. 8018–8034, Oct. 2017.

[5] Z. Zhang, Z. Li, M. P. Kazmierkowski, J. Rodríguez, and R. Kennel, "Robust predictive control of 3-level NPC back-to-back power converter PMSG wind turbine systems with revised predictions," *IEEE Trans. Power Electron.*, vol. 33, no. 11, pp. 9588–9598, Nov. 2018.

[6] L. Tarisciotti, G. L. Calzo, A. Gaeta, P. Zanchetta, F. Valencia, and D. Sáez, "A distributed model predictive control strategy for back-to-back converters," *IEEE Trans. Ind. Electron.*, vol. 63, no. 9, pp. 5867–5878, Sep. 2016.

[7] S. Thielemans, T. J. Vyncke, and J. Melkebeek, "Weight factor selection for model-based predictive control of a four-level flying-capacitor inverter," *IET Power Electron.*, vol. 5, no. 3, pp. 323–333, Mar. 2012.

[8] M. Novak, U. M. Nyman, T. Dragicevic, and F. Blaabjerg, "Analytical design and performance validation of finite set MPC regulated power converters," *IEEE Trans. Ind. Electron.*, vol. 66, no. 3, pp. 2004–2014, Mar. 2019.

[9] T. Dragicevic and M. Novak, "Weighting factor design in model predictive control of power electronic converters: An artificial neural network approach," *IEEE Trans. Ind. Electron.*, to be published, doi: 10.1109/TIE.2018.2875660.

[10] L. M. A. Caseiro, A. M. S. Mendes, and S. M. A. Cruz, "Dynamically weighted optimal switching vector model predictive control of power converters," *IEEE Trans. Ind. Electron.*, vol. 66, no. 2, pp. 1235–1245, Feb. 2019.

[11] Y. Zhang and H. Yang, "Two-vector-based model predictive torque control without weighting factors for induction motor drives," *IEEE Trans. Power Electron.*, vol. 31, no. 2, pp. 1381–1390, Feb. 2016.

[12] Y. Zhang and H. Yang, "Model-predictive flux control of induction motor drives with switching instant optimization," *IEEE Trans. Energy Convers.*, vol. 30, no. 3, pp. 1113–1122, Sep. 2015.

[13] F. Donoso, A. Mora, R. Cardenas, A. Angulo-Cárdenas, D. Sáez, and M. Rivera, "Finite-set model predictive control strategies for a 3L-NPC inverter operating with fixed switching frequency," *IEEE Trans. Ind. Electron.*, vol. 65, no. 5, pp. 3954–3965, May 2018.

[14] P. Acuña, L. Morán, M. Rivera, R. Aguilera, R. Burgos, and V. G. Agelidis, "A single-objective predictive control method for a multivariable single-phase three-level NPC converter-based active power filter," *IEEE Trans. Ind. Electron.*, vol. 62, no. 7, pp. 4598–4607, Jul. 2015.

[15] C. A. Rojas, J. Rodriguez, F. Villarroel, J. R. Espinoza, C. A. Silva, and M. Trincado, "Predictive torque and flux control without weighting factors," *IEEE Trans. Ind. Electron.*, vol. 60, no. 2, pp. 681–690, Feb. 2013.
[16] V. P. Muddineni, A. K. Bonala, and S. R. Sandepudi, "Enhanced weighting factor selection for predictive torque control of induction motor drive based on VIKOR method," *IET Electric Power Appl.*, vol. 10, no. 9, pp. 877–888, 2016.
[17] S. A. Davari, D. A. Khaburi, and R. Kennel, "An improved FCS-MPC algorithm for an induction motor with an imposed optimized weighting factor," *IEEE Trans. Power Electron.*, vol. 27, no. 3, pp. 1540–1551, Mar. 2012.
[18] D. K. Choi and K. B. Lee, "Dynamic performance improvement of AC/DC converter using model predictive direct power control with finite control set," *IEEE Trans. Ind. Electron.*, vol. 62, no. 2, pp. 757–767, Feb. 2015.
[19] O. Machado, P. Martín, F. J. Rodríguez, and E. J. Bueno, "A neural network-based dynamic cost function for the implementation of a predictive current controller," *IEEE Trans. Ind. Inform.*, vol. 13, no. 6, pp. 2946–2955, Dec. 2017.
[20] X. Li, H. Zhang, M. B. Shadmand, and R. S. Balog, "Model predictive control of a voltage-source inverter with seamless transition between islanded and grid-connected operations," *IEEE Trans. Ind. Electron.*, vol. 64, no. 10, pp. 7906–7918, Oct. 2017.
[21] V. Yaramasu, B. Wu, and J. Chen, "Model-predictive control of grid-tied four-level diode-clamped inverters for high-power wind energy conversion systems," *IEEE Trans. Power Electron.*, vol. 29, no. 6, pp. 2861–2873, Jun. 2014.
[22] P. Cortes, G. Ortiz, J. I. Yuz, J. Rodriguez, S. Vazquez, and L. G. Franquelo, "Model predictive control of an inverter with output LC filter for UPS applications," *IEEE Trans. Ind. Electron.*, vol. 56, no. 6, pp. 1875–1883, Jun. 2009.

Luís M. A. Caseiro (S'12–M'17) received the M.Sc. and Ph.D. degrees in electrical engineering from the University of Coimbra, Coimbra, Portugal, in 2012 and 2017, respectively.

He is currently an Assistant Researcher with the Instituto de Telecomunicações, Coimbra. His research interests are focused on high-quality and high-reliability power electronics converters, with special emphasis on fault diagnosis, fault tolerance and digital control techniques.

André M. S. Mendes (S'95–M'05) received the Electrical Engineering Diploma, the M.Sc. and Dr. Eng. degrees in electrical engineering from the University of Coimbra, Coimbra, Portugal in 1993, 1998, and 2005, respectively.

He has been with the Department of Electrical and Computer Engineering, University of Coimbra, where he is currently an Assistant Professor and the Director of the Power Electronics Laboratory. His teaching interests cover electric machines and power electronics, and his research interests are focused on power quality, fault diagnosis and fault tolerance of electric drives, and power electronic converters.

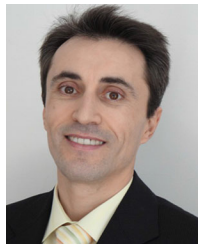

Sérgio M. A. Cruz (S'96–M'04–SM'16) received the Electrical Engineering Diploma, the M.Sc. and Dr.Eng. degrees in electrical engineering from the University of Coimbra, Coimbra, Portugal, in 1994, 1999, and 2004, respectively.

He is with the Department of Electrical and Computer Engineering, University of Coimbra, where he is currently an Assistant Professor and the Director of the Electric Machines Laboratory. His teaching and research interests include power transformers, rotating electric machines, electric drives, and power electronic converters, with special emphasis on fault diagnosis, fault tolerance, and digital control.